PD Based Fuzzy Sliding Mode Control of A Wheelchair Exoskeleton Robot.

Teng, Long; Gull, Muhammad Ahsan; Bai, Shaoping

Published in:
I E E E - A S M E Transactions on Mechatronics

DOI (link to publication from Publisher):
10.1109/TMECH.2020.2983520

Publication date:
2020

Document Version
Accepted author manuscript, peer reviewed version

This article has been accepted for publication in a future issue of this journal, but has not been fully edited. Content may change prior to final publication. Citation information: DOI 10.1109/TMECH.2020.2983520, IEEE/ASME Transactions on Mechatronics

PD Based Fuzzy Sliding Mode Control of A Wheelchair Exoskeleton Robot

Long Teng, *Member*, *IEEE*, Muhammad Ahsan Gull, *Student Member*, *IEEE*, and Shaoping Bai, *Senior Member*, *IEEE*

***Abstract*—Wheelchair upper-limb exoskeletons can offer a new paradigm to assist people with neuromuscular dysfunction in their activities of daily living (ADLs) such as eating and drinking. A key challenge in their control is to ensure safe and comfortable interaction between the human upper limb and exoskeleton. Compared with industrial manipulators, exoskeletons suffer severe kinematic and dynamic uncertainties and external disturbances. Therefore, the selection of optimal control methods that can address the aforementioned challenge is required. In this paper, a method combining PD control, sliding mode control, and fuzzy logic control, i.e., PD based fuzzy sliding mode control, is developed to deal with unmodeled dynamics and external disturbances in the human-exoskeleton system. The sliding mode control can be generally divided by the equivalent control law and the switching control law. For the basic equivalent control part, it adopts the PD controller due to its simplicity in controller design and parameter tuning. For the switching control part, it is replaced by fuzzy logic control to eliminate the chattering of control input such that the smooth motion of the system is achieved. Simulation and experiment results are provided to show the effectiveness of the proposed control method.**

***Index Terms*—Wheelchair upper-limb exoskeleton robot, sliding mode control (SMC), fuzzy logic control, trajectory tracking, gravity compensation, ADL assistance.**

I. Introduction

An exoskeleton is a robotic system attached to a human subject to provide supplementary power or regain motor functions [1]. Exoskeletons have been used for different applications such as rehabilitation [2], assistance of activities of daily living (ADLs) [3], surgery [4], and workplace support [5] and so on. Among existing different kinds of exoskeleton robots, wheelchair upper-limb exoskeletons combine the advantages of wheelchairs and upper-limb exoskeletons for rehabilitation and motion assistance. With this type of exoskeletons, patients or users do not need to bear the heavyweight of wearing exoskeletons yet get motion assistance as needed. For exoskeletons toward these applications, how to ensure safe and comfortable physical human-robot interaction is a critical issue for the controller design. Compared with manipulators, exoskeletons acquire several unique properties. Firstly, links of an exoskeleton have to be adjustable so that it can be attached to users with different anthropomorphic parameters. As a result, it introduces kinematic and dynamic uncertainties into the control system for the exoskeleton. Secondly, exoskeletons are usually used in different modes. For example, rehabilitation exoskeletons can work in three modes in general: passive (or assistive), active, and resistive modes. Specifically, passive assistance is ideal for early-stage rehabilitation, where the exoskeleton usually performs trajectory tracking to assist the patients in their ADLs, such as reaching, grasping, and eating. A controller that is able to account for these factors is needed.

A review of control strategies for upper-limb exoskeletons for rehabilitation can be found in [6]. Regarding the position tracking problem, many control approaches, such as proportional-integral-derivative (PID) controller [7], adaptive control [8], fuzzy control [9], neural network-based control [10], model predictive control [11], sliding mode control (SMC) [12] and so on, have been proposed so far. In SMC, a sliding surface comprised of a combination of error signals is adopted such that the tracking error is reduced to a certain acceptable level, and the stability of the closed-loop system is guaranteed [12]. An advantage of SMC is its ability to deal with systems with extensive disturbances and uncertainties. Furthermore, SMC has a simple control structure with good transient performance [13]. However, classical SMC usually suffers significant oscillations of the control law due to frequent and abrupt switchings, which cause the chattering phenomenon of the actuator that should be avoided in practical applications.

In [14], [15], combinations of adaptive control with sliding mode control, i.e., adaptive sliding mode control (ASMC), were studied to achieve robust trajectory tracking against disturbances and uncertainties and eliminate the chattering in the meanwhile. The combination of fuzzy control and SMC, i.e., fuzzy sliding mode control (FSMC), provides an alternative approach for improving control performance of trajectory tracking. Fuzzy logic control has a simple representation that is strongly supported by the heuristic nature of human reasoning and applicable for modeling and control of nonlinear and complex systems [16]–[23]. To acquire smooth control signals in variable structure systems, a method of bandwidth low-pass filter with fuzzy tuning was reported in [24]. Fuzzy logic controller to reduce the chattering in SMC by replacing the discontinuous switching control law was studied in [25].

A few studies of FSMC for exoskeleton robots were re-

This work was supported by Innovation Fund Denmark through the REMAP project, and the EU AAL Programme through the AXO-SUIT project. (Corresponding authors: Long Teng & Shaoping Bai.)

L. Teng, MA. Gull and S. Bai are with the Department of Materials and Production, Aalborg University, Aalborg 9220, Denmark (Email: teng@mp.aau.dk; mag@mp.aau.dk; shb@mp.aau.dk).

This article has been accepted for publication in a future issue of this journal, but has not been fully edited. Content may change prior to final publication. Citation information: DOI 10.1109/TMECH.2020.2983520, IEEE/ASME Transactions on Mechatronics

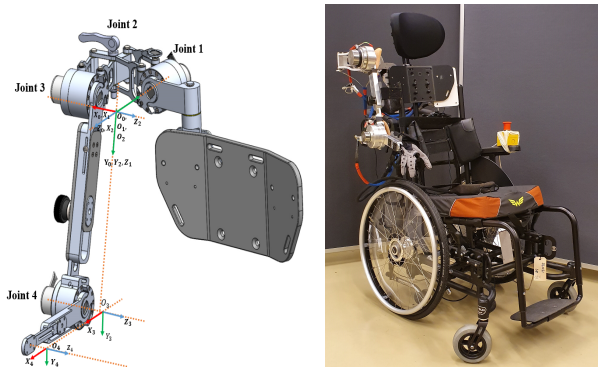

(a) (b)

Fig. 1. Overview of the wheelchair exoskeleton. (a) Exoskeleton mechanical model. The red, green, blue lines represent the X, Y, Z axes, respectively. (b) Wheelchair exoskeleton with the robotic glove. The control board is mounted on the back of the wheelchair. The red button is the power-off button in case of an emergency.

ported. In [26], fuzzy sliding mode admittance control was investigated to enable the active participation of the patients; however, it depends on the dynamic modeling of exoskeleton and human, which may be inaccurate due to the modeling errors. Besides, it only applies to a 1-DOF elbow exoskeleton, which cannot provide enough range of motion (ROM) for ADLs. In [27], FSMC with a new sliding surface was proposed for a 7-DOF upper-limb exoskeleton. However, only simulation results were reported. As such, controller development and experiment validation of multi-DOF exoskeletons for practical ADL tasks are needed.

In this paper, a control method combining PD control, SMC, fuzzy logic control, and gravity compensation is proposed for a 4-DOF wheelchair upper-limb exoskeleton robot. The contributions of this work are summarized as follows:

1) The proposed control method combines PD control, SMC, fuzzy logic control, to achieve high position tracking performance for upper-limb exoskeleton. The method inherits the advantages of the fast response and enhanced stability from PD control and the robustness from SMC against system uncertainties and external disturbances. Furthermore, the chattering phenomenon caused by classical sliding mode control is eliminated by combining fuzzy logic control and SMC.

2) In practical applications, it is usually very difficult to achieve full and precise gravity compensation of the human-exoskeleton system. By combining different control approaches such as partial gravity compensation and the PD based FSMC, the new method can achieve tracking control performance similar to that of a combination of full gravity compensation and FSMC. As a result, full and precise gravity compensation is not necessary for the proposed control method.

Experiment validation which shows that the proposed control method is appropriate for performing real-world ADL tasks such as eating/drinking is another contribution of this work.

The rest of this paper is organized as follows. A wheelchair upper-limb exoskeleton is introduced in Section II. Its kinematics is also modeled to fulfill ADL tasks in operational space. FSMC control architecture is investigated in Section III. The SMC is introduced at first, based on which, the FSMC algorithm is developed. Section IV presents the simulation results against other control methods for a 2-DOF manipulator. The controller implementation followed by the experiment results on the wheelchair exoskeleton is illustrated in Section V. Subsequently, comparisons among different control methods and scenarios are also presented. Finally, conclusions and future directions are given in Section VI.

TABLE I
DENAVIT-HARTENBERG (DH) PARAMETERS

Links	α_i	a_i	d_i	θ_i
1	$-\pi/2$	0	0	θ_1
2	$\pi/2$	0	0	θ_2
3	0	L_u	0	θ_3
4 (wrist)	0	L_f	0	θ_4

II. A WHEELCHAIR EXOSKELETON ROBOT

A. Mechanical Model

Fig. 1 presents a wheelchair-mounted exoskeleton developed at Aalborg University, Denmark. The wheelchair exoskeleton system consists of two subsystems: an upper-limb exoskeleton and a soft glove. For the upper-limb exoskeleton, there are 3 DOFs in the shoulder mechanism responsible for shoulder adduction/abduction (joint 1 in Fig. 1(a)), shoulder internal/external rotation (joint 2), and shoulder flexion/extension (joint 3). In addition, the elbow joint supports elbow flexion/extension (joint 4). It is noted that joint 2 for shoulder internal/external rotation is a passive joint. The soft robotic glove is a commercial product from BioServo that can be directly worn on the user's hand and improve the grasping capability (see Fig. 1(b)).

The wheelchair upper-limb exoskeleton is adapted from [28], where it was originally used for human power amplification. In this work, the exoskeleton is mounted on a wheelchair to assist users suffering from neuro-muscular dysfunction. For these users, they cannot generate enough muscle strength to hold and carry even a lightweight object. Thus, a passive rehabilitation strategy is adopted to provide full support to the arm motion. In the current setup, the passive joint 2 is fixed to 90° to allow for precise position tracking. In fact, by fixing joint 2, the exoskeleton can still perform basic tasks like reaching, grasping, and eating.

B. Kinematics

The kinematic model of the exoskeleton is developed with Denavit-Hartenberg (DH) parameters defined in Table I, where L_u and L_f represent the lengths of the upper-arm and forearm links, respectively. Based on the DH parameters, the transformation matrix is given by

$$\mathrm{T}_{i-1,i} = \begin{bmatrix} c\theta_i & -s\theta_i & 0 & a_i \\ s\theta_i c\alpha_i & c\theta_i c\alpha_i & -s\alpha_i & -s\alpha_i d_i \\ s\theta_i s\alpha_i & c\theta_i s\alpha_i & c\alpha_i & c\alpha_i d_i \\ 0 & 0 & 0 & 1 \end{bmatrix} \quad (1)$$

This article has been accepted for publication in a future issue of this journal, but has not been fully edited. Content may change prior to final publication. Citation information: DOI 10.1109/TMECH.2020.2983520, IEEE/ASME Transactions on Mechatronics

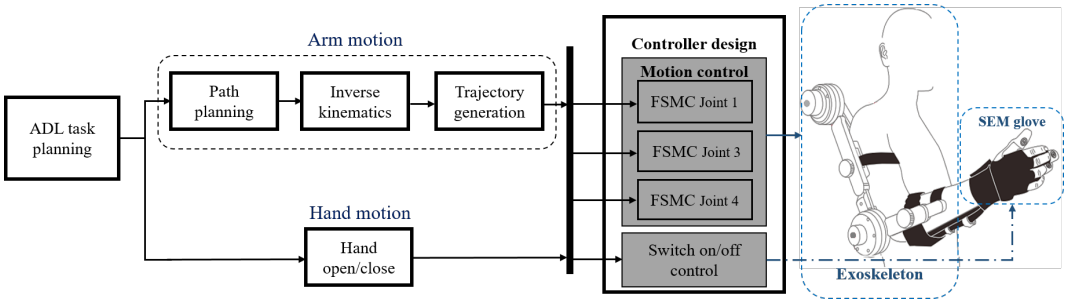

Fig. 2. Overall system control architecture. The ADL tasks are predefined. The FSMC algorithm is designed for the control of each joint. The robotic glove adopts switch on/off control.

where s and c represent the sine and cosine functions, respectively.

The forward kinematics is solved by calculating the overall transformation matrix

$$\mathrm{T}_{0,5} = \begin{bmatrix} m_{11} & m_{12} & m_{13} & n_{14} \\ m_{21} & m_{22} & m_{23} & n_{24} \\ m_{31} & m_{32} & m_{33} & n_{34} \\ 0 & 0 & 0 & 1 \end{bmatrix} \tag{2}$$

where all entries are given in Appendix I.

The inverse kinematics is calculated from the transformation matrix (2). The result is presented as solving the following equations in sequence,

$$\theta_2 = \pm \arccos(m_{33}) \tag{3}$$

$$n_{14}c\theta_1 + n_{24}s\theta_1 + n_{34}\cot\theta_2 = 0 \tag{4}$$

$$2M_1L_uc\theta_3 + 2M_2L_us\theta_3 + {L_u}^2 - {L_f}^2 + {M_1}^2 + {M_2}^2 = 0 \tag{5}$$

$$\theta_4 = \arctan 2(\frac{M_2 + L_us\theta_3}{-L_f}, \frac{M_1 + L_uc\theta_3}{-L_f}) - \theta_3 \tag{6}$$

where

$$\begin{cases} M_1 = \dfrac{n_{34}}{s\theta_2} \\ M_2 = n_{14}s\theta_1 - n_{24}c\theta_1 \end{cases} \tag{7}$$

Equations (4), (5) and (6) can be solved using the algebraic methods presented in [29]. The $\arctan 2$ function denotes the 2-argument arctangent function.

It is noted that the FSMC approach used in this work is free of modeling of system dynamics, thus the dynamic model of the exoskeleton can be ignored.

C. Exoskeleton Control System

The architecture of the control system is demonstrated in Fig. 2. The control system includes ADL task planning, path planning, inverse kinematics computation, trajectory generation, and motion controller design. Control signals are sent to the exoskeleton and the robotic glove to support ADL tasks.

The embedded control system consists of an Arduino Due microprocessor, motors, motor drivers, and encoders. A graphic user interface (GUI) is also developed with MATLAB on a laptop, through which the user can easily select control mode, tune control parameters, send high-level control commands, and check the running data. The serial communication is adopted for the communication between the Arduino microprocessor and laptop. The low-level position control algorithm, the calculation of forward/inverse kinematics, and the trajectory generation are implemented in the Arduino microprocessor.

III. FSMC Approach

A. Sliding Mode Control Architecture

The dynamic model of a multi-link serial robotic manipulator can be expressed by the following equation

$$M(q)\ddot{q} + C(q,\dot{q}) + \tau_g = \tau \tag{8}$$

where q, $\dot{q}$, $\ddot{q}$, are the vectors of joint positions, velocities, and accelerations of the robot, respectively. $M(q)$ denotes the inertial matrix which is symmetric and bounded positive definite, $C(q,\dot{q})$ denotes the torque vector induced by Coriolis and centrifugal forces, τ_g is the torque vector induced by gravitational forces, τ is the control input torque vector. Although the FSMC developed in this work is free of dynamic modeling, the dynamic model (8) is still provided here to represent the typical robotic systems.

In this work, a trajectory tracking control problem has been investigated, where the joint position q is required to track the desired trajectories q_d. $e = q - q_d$ denotes the position tracking error and let $x_1 = e$, $x_2 = \dot{e}$, thus a new state-space model is generated as follows

$$\begin{cases} \dot{x}_1 = x_2 \\ \dot{x}_2 = -u \end{cases} \tag{9}$$

where u is a new control input. In what follows, the control problem of the system (9) is considered rather than the original system (8).

For the aforementioned system (9), the SMC method is investigated, with which a sliding surface is chosen as follows

$$S(t) = \dot{e}(t) + k_1 \int_0^t e(\varphi)d\varphi + k_2 e(t) \tag{10}$$

where k_1 and k_2 are gains of the sliding surface. φ represents the time instant. The SMC requires that when the system trajectories reach the sliding surface $S(t)$, the tracking error and its derivative will converge to zero.

For system (9) with the sliding surface (10), the control law is defined as follows

$$u = u_{eq} + u_s \tag{11}$$

where u_{eq} and u_s are the equivalent controller and the switching controller, respectively. u_{eq} is used to keep the system on the sliding surface, based on which, the derivative of the sliding surface must be equal to zero, that is

$$\begin{aligned} \dot{S}(t) &= \ddot{e}(t) + k_1 e(t) + k_2 \dot{e}(t) \\ &= \dot{x}_2 + k_1 x_1 + k_2 x_2 \\ &= -u_{eq} + k_1 x_1 + k_2 x_2 \\ &= 0 \end{aligned} \tag{12}$$

From (12), u_{eq} is derived as

$$\begin{aligned} u_{eq} &= k_1 x_1 + k_2 x_2 \\ &= k_1 e + k_2 \dot{e} \end{aligned} \tag{13}$$

Theorem 1. Consider system (9) with sliding surface S defined by (10), $u = u_{eq} + \rho \text{sgn}(S)$ is a stabilizable controller with ρ being a positive constant.

Proof: Consider the following Lyapunov function

$$V(S(t)) = \tfrac{1}{2} S^T S \tag{14}$$

Its derivative is

$$\begin{aligned} \dot{V}(S(t)) &= \dot{S}^T S \\ &= (-u + k_1 x_1 + k_2 x_2)^T S \\ &= (-u_{eq} - u_s + k_1 x_1 + k_2 x_2)^T S \\ &= (-\rho \text{sgn}(S))^T S \\ &< 0 \end{aligned} \tag{15}$$

Thus, the system (9) is stabilizable with the controller defined in Theorem 1. The proof is complete.

From Theorem 1 and (11), the switching controller u_s is acquired as

$$u_s = \rho \text{sgn}(S) \tag{16}$$

In above switching controller, u_s switches its directions with $S(t)$ to ensure closed-loop stability, with ρ representing the amplitude of u_s. However, the performance of the switching controller highly relies on the selection of ρ, a small value of ρ usually results in very weak switching control actions which will reduce the tracking performance; on the contrary, a big value of ρ leads to too strong switching control actions which usually cause severe chattering phenomenon of the actuator. To overcome this dilemma, the T-S fuzzy approach is introduced to achieve a smooth control law along the sliding surface to reduce its amplitude sensitivity with the increase of ρ. As a result, the tracking performance is improved and the chattering phenomenon is suppressed in the meantime.

B. Fuzzy Sliding Mode Control

Based on the aforementioned SMC method, the following fuzzy rules are considered for the control input $u(t)$ in Theorem 1:

Rule 1: IF $S(t) > 0$
THEN $u(t)$ is positive,

$$u(t) = u_1 = u_{eq} + \rho \tag{17}$$

Rule 2: IF $S(t) < 0$
THEN $u(t)$ is negative,

$$u(t) = u_2 = u_{eq} - \rho \tag{18}$$

where $S(t)$ is the premise variable of the fuzzy rules and the following membership functions are selected,

$$\begin{cases} \mu_1(S(t)) = \frac{1}{1+e^{-\lambda S(t)}} & if\ S(t) > 0 \\ \mu_2(S(t)) = \frac{1}{1+e^{\lambda S(t)}} & if\ S(t) < 0 \end{cases} \tag{19}$$

where λ is a positive scalar, One can easily get that $\mu_1(S(t))$, $\mu_2(S(t)) > 0$, and $\mu_1(S(t)) + \mu_2(S(t)) = 1$.

(19) shows that different values for λ lead to different membership functions. Fig. 3 illustrates the membership functions with $\lambda = 1$ and $\lambda = 5$, respectively.

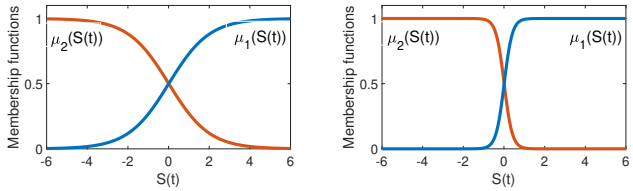

(a) $\lambda = 1$ (b) $\lambda = 5$

Fig. 3. Membership functions with different values of λ.

Finally, the control input is formulated by the following equation

$$u(t) = \mu_1(S(t))u_1 + \mu_2(S(t))u_2 \tag{20}$$

The implementation of the fuzzy sliding mode control algorithm for trajectory tracking of each joint is summarized in pseudo-code manner shown below.

Algorithm: Fuzzy Sliding Mode Control for Each Joint.

Given:

- Sampling time: T_s
- User-selected parameters: k_1, k_2, ρ, λ
- Original desired trajectory: $q_d(k)$

Initialize:

- $e(0) = 0$

$k \leftarrow 1$

Repeat:

- $e(k) = q_d(k) - q(k)$, $\dot{e}(k) = \frac{e(k)-e(k-1)}{T_s}$, $\sum_0^k e = \sum_0^{k-1} e(j) + e(k)T_s$
- $S(k) = \dot{e}(k) + k_1 e(k) + k_2 \sum_0^k e(j)$
- $u_{eq}(k) = k_1 \dot{e}(k) + k_2 e(k)$
- $u_1(k) = u_{eq}(k) + \rho$, $u_2(k) = u_{eq}(k) - \rho$
- $\mu_1(S(k)) = \frac{1}{1+e^{-\lambda(S(k))}}$, $\mu_2(S(k)) = \frac{1}{1+e^{\lambda(S(k))}}$
- $u(k) = \mu_1(S(k))u_1(k) + \mu_2(S(k))u_2(k)$
- $e(k-1) \leftarrow e(k)$, $\sum_0^{k-1} e(j) \leftarrow \sum_0^k e(j)$
- $k \leftarrow k + 1$.

From (13) it can be seen that the equivalent controller u_{eq} has the same representation as the PD control. Therefore, u_{eq} can simply be decided by PD control, i.e., k_1 and k_2 can be tuned following existing methods used for PD control. Moreover, from (17) and (18), the FSMC can be regarded as

PD control if ρ is selected as 0. Based on the aforementioned statements, the parameter-tuning method for the PD-based FSMC is summarized below.

Control parameter tuning:

1: Select PD control strategy, i.e., let $\rho = 0$, and tune PD control using classical Nichols-Ziegler method, upon which control gains k_1 and k_2 are obtained.

2: Select the FSMC control strategy, i.e., let $\rho > 0$, and use the same gains k_1 and k_2 acquired from the above PD control. Then increase ρ gradually from a smaller value in tuning until an optimum trajectory tracking is achieved.

IV. FSMC Simulation

In this section, the FSMC performance is evaluated by simulation. For comparison purposes, two other methods including the classic PD control and the adaptive sliding mode control (ASMC) introduced in [15] are executed as well. The 2-DOF manipulator in [15] is adopted in this work, see Fig. 9 in Appendix II. The dynamic model of the 2-DOF manipulator is presented below.

$$\begin{aligned}\begin{bmatrix}\tau_1\\ \tau_2\end{bmatrix} &= \begin{bmatrix}M_{11} & M_{12}\\ M_{21} & M_{22}\end{bmatrix}\begin{bmatrix}\ddot{q}_1\\ \ddot{q}_2\end{bmatrix} + \\ &\begin{bmatrix}-h\dot{q}_2 & -h(\dot{q}_1+\dot{q}_2)\\ h\dot{q}_1 & 0\end{bmatrix}\begin{bmatrix}\dot{q}_1\\ \dot{q}_2\end{bmatrix} + \begin{bmatrix}F_{c1} & 0\\ 0 & F_{c2}\end{bmatrix} \\ &\begin{bmatrix}\mathrm{sgn}(\dot{q}_1)\\ \mathrm{sgn}(\dot{q}_2)\end{bmatrix} + \begin{bmatrix}v_1 & 0\\ 0 & v_2\end{bmatrix}\begin{bmatrix}\dot{q}_1\\ \dot{q}_2\end{bmatrix} + \begin{bmatrix}d_1(t)\\ d_2(t)\end{bmatrix}\end{aligned} \tag{21}$$

where $M_{11} = a_1 + 2a_3\cos(q_2) - 2a_4\sin(q_2)$, $M_{12} = M_{21} = a_2 + a_3\cos(q_2) + a_4\sin(q_2)$, $M_{22} = a_2$, $h = a_3\sin(q_2) - a_4\cos(q_2)$. The system parameters are provided in Appendix II and more details can be found in [15].

Control parameters for the three control methods are given as follows:

PD control: The proportional and differential gains are selected as $\begin{bmatrix}k_p & k_d\end{bmatrix} = \begin{bmatrix}600 & 400\end{bmatrix}$, $\begin{bmatrix}k_p & k_d\end{bmatrix} = \begin{bmatrix}600 & 400\end{bmatrix}$, respectively, for the two joints.

ASMC [15]: The overall controller is comprised of three parts: the equivalent control u_{eq}, the PID control u_{PID}, and the adaptive control $\hat{u}_p$. Moreover, it relies on the system dynamic model. The control parameters are chosen the same as in [15].

FSMC: Since the proposed FSMC control is based on the PD control, the equivalent controller u_{eq} can be simply selected as same as the PD controller, thus $\begin{bmatrix}k_1 & k_2\end{bmatrix} = \begin{bmatrix}600 & 400\end{bmatrix}$ for joint 1, $\begin{bmatrix}k_1 & k_2\end{bmatrix} = \begin{bmatrix}600 & 400\end{bmatrix}$ for joint 2. For the switching control u_s, $\rho_1 = \rho_2 = 5$. Consider the fuzzy membership function, $\lambda_1 = \lambda_2 = 200$.

The reference trajectories q_{ref} for the two joints are [15]

$$q_{ref} = \begin{bmatrix}\pi/6\,(1-\cos(1.5\pi t) + \sin(\pi t))\\ \pi/6\,(1-\cos(2\pi t) + \sin(1.5\pi t))\end{bmatrix} \tag{22}$$

The simulation results of the above three control strategies for the system without and with disturbances are shown in Figs. 4 and 5, respectively. The disturbance signals are selected as $100sin(1.6\pi t)$ for both joints, see Fig. 5. Comparing Fig. 4 and Fig. 5, from the tracking errors of joints one can observe that the tracking performance of PD deteriorated severely when disturbances were involved. Without disturbances, the amplitudes of errors for both joints by PD are about 0.04rad; with disturbances, the amplitudes of errors for both joints increase to 0.09rad. Similar results are obtained with the ASMC algorithm. Regardless of the severe oscillations in the beginning (0-0.5s), the error amplitudes for the two joints were found to be 0.0023rad and 0.0048rad without any external disturbance. Whereas, by adding the disturbances, the error amplitudes for the two joints were observed to be 0.0061rad and 0.01rad, respectively. In comparison with PD and ASMC, Fig. 4 and Fig. 5 show that the tracking errors were significantly reduced by FSMC in both without/with disturbance cases, which indicates that FSMC achieves the best trajectory tracking performance against the other two approaches.

Furthermore, from the view of the control input torque shown in Figs. 4 and 5, there are severe oscillations of the control torque with ASMC at the beginning time. The oscillating phenomenon was also observed in [15], which is not desirable for the actuators and physical human-robot interaction in practical ADL tasks. On the contrary, the control torque generated by FSMC is very smooth.

V. Control Implementation In Exoskeleton

In this section, the proposed FSMC is implemented in the wheelchair exoskeleton. In connection with the implementation, the gravity compensation technique is introduced in combination with the FSMC approach and then the experiment results are provided.

A. Gravity Compensation Technique

The gravity torque τ_g in the dynamic system (8) can be compensated in the controller design, which can further improve the motion control performance. The gravity compensation technique can be formulated as the following equation,

$$\tau_g = \sum_{s}^{N} p_s \times (m_s g) \tag{23}$$

where p_s represents the displacement vector from the joint to the center of mass of segment s, m_s represents the mass of the segment, g is the gravitational constant vector, with all vectors being in the global coordinate system. PD control with gravity compensation for motion control has been extensively investigated and a closed-loop stability analysis can be seen in [30]. The mechanical properties of the exoskeleton and the anthropomorphic parameters of a human upper-limb for gravity compensation are shown in Table IV in Appendix III, where we used approximate values for the length and the weight of the human arm.

From (20) and (23), the method of combining PD based FSMC with gravity compensation is finally expressed as

$$\begin{aligned}\hat{u}(t) &= u(t) + \tau_g\\ &= \mu_1(S(t))u_1 + \mu_2(S(t))u_2 + \tau_g\end{aligned} \tag{24}$$

where $\hat{u}(t)$ is the final input of control torque.

This article has been accepted for publication in a future issue of this journal, but has not been fully edited. Content may change prior to final publication. Citation information: DOI 10.1109/TMECH.2020.2983520, IEEE/ASME Transactions on Mechatronics

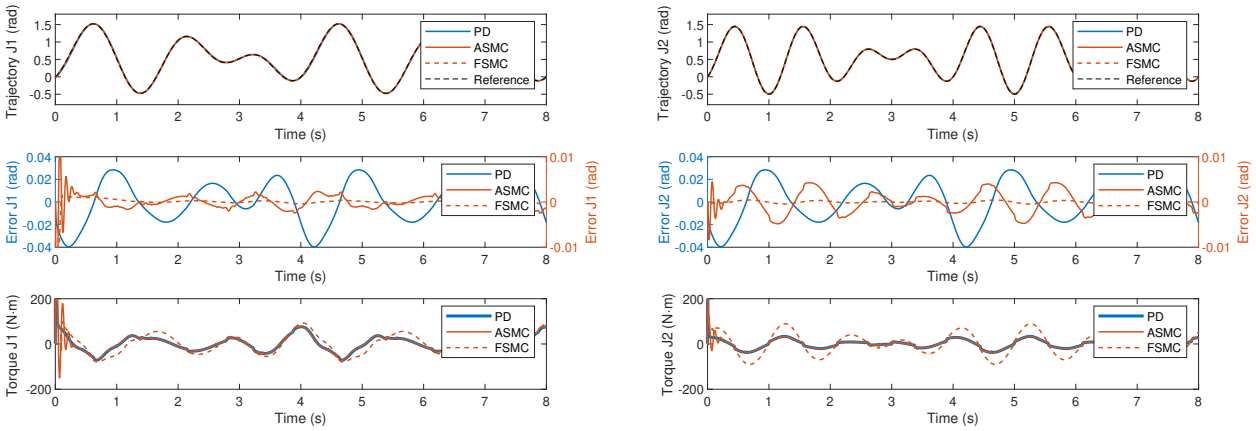

(a) Joint 1 (b) Joint 2

Fig. 4. Simulation results of a 2-DOF manipulator without external disturbances.

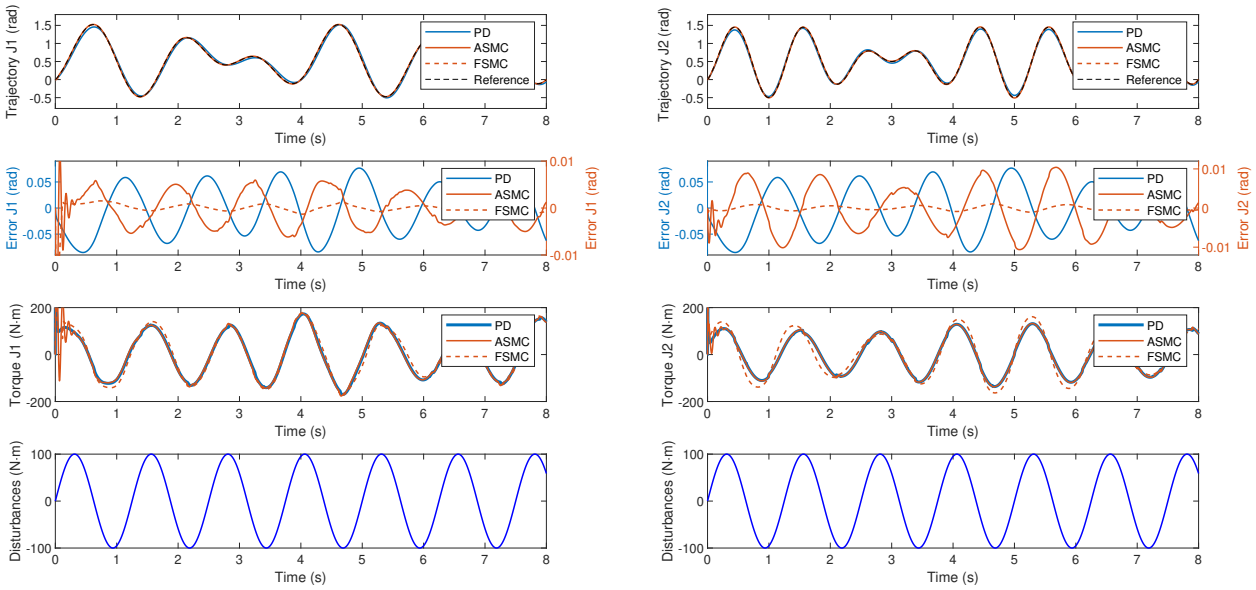

(a) Joint 1 (b) Joint 2

Fig. 5. Simulation results of a 2-DOF manipulator with external disturbances.

It should be noted that it is difficult to achieve accurate gravity compensation for the control of exoskeleton robots due to several limitations from the exoskeleton, the human subject, and the payload:

1) It is difficult to calculate a precise gravity torque due to the irregular shapes and center of mass (COM) of the exoskeleton links and those of human subjects. Additionally, it is almost impossible to measure human body properties in practical applications. Instead, we can only approximate these properties of the subjects.

2) In practical applications, the length of the exoskeleton links should be adjusted according to the length of human upper arms and forearms. As a consequence, the gravity torque depends upon the exoskeleton link length and user upper limb physiology.

3) The gravity torque (or disturbance torque) induced by the payload is usually time-varying even in a specific ADL task. Moreover, it is uncertain among different ADL tasks due to the change of payload.

As our experiment results will show, the FSMC method can achieve high trajectory tracking performance even though the gravity torque is partially compensated.

This article has been accepted for publication in a future issue of this journal, but has not been fully edited. Content may change prior to final publication. Citation information: DOI 10.1109/TMECH.2020.2983520, IEEE/ASME Transactions on Mechatronics

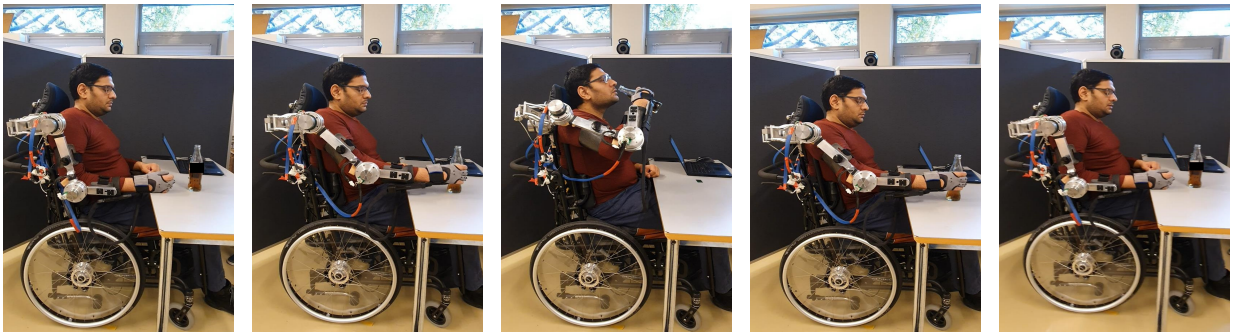

(a) The initial position. (b) The "grasping" position. (c) The "drinking" position. (d) The "release" position. (e) The initial position.

Fig. 6. Demonstrations of a drinking task: from time 0 to 8s, the exoskeleton stays at the initial position; from 8s to 13s, the exoskeleton moves to the "grasping" position; from 13s to 18s, it takes 5s for grasping of the object with the robotic glove; from 18s to 28s, the exoskeleton moves toward the human mouth (the "eating" position); from 28s to 43s, the exoskeleton stays at the eating position to allow drinking of water; from 43s to 53s the exoskeleton will return to the "release" position and then release the object from 53s to 58s; finally, the exoskeleton will go back to the initial position.

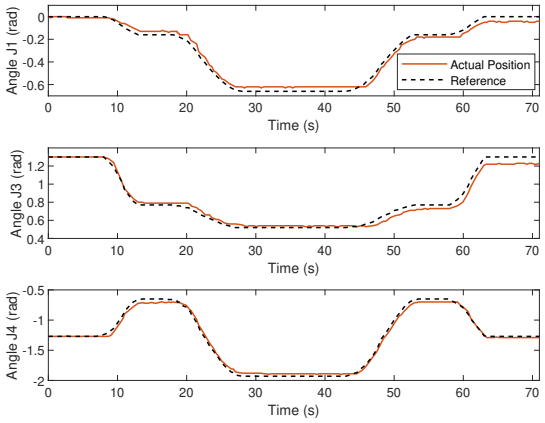

(a) PD with full gravity compensation

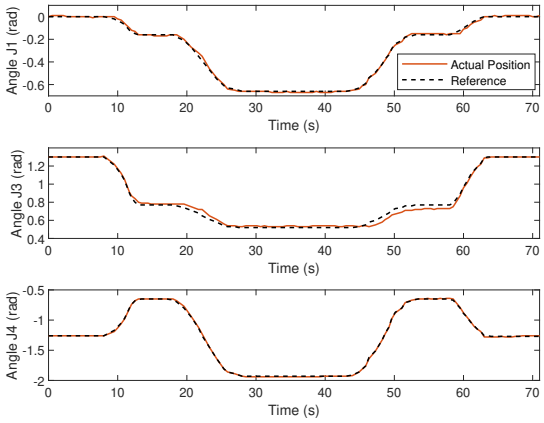

(b) FSMC

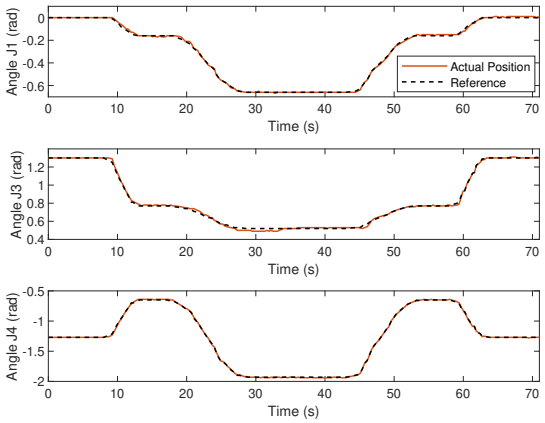

(c) FSMC with partial gravity compensation

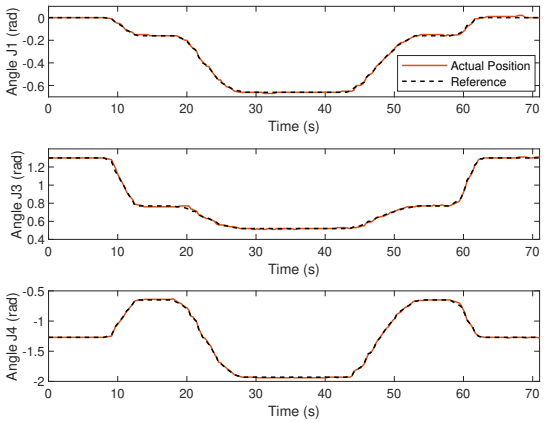

(d) FSMC with full gravity compensation

Fig. 7. Trajectory tracking control performance for a drinking task by (a) PD with full gravity compensation, (b) FSMC, (c) FSMC with partial gravity compensation, and (d) FSMC with full gravity compensation.

This article has been accepted for publication in a future issue of this journal, but has not been fully edited. Content may change prior to final publication. Citation information: DOI 10.1109/TMECH.2020.2983520, IEEE/ASME Transactions on Mechatronics

TABLE II
CONTROLLER PARAMETERS.

Control Algorithm	Controller parameters	Joint 1	Joint 3	Joint 4
PD	k_p	11	18	11
	k_d	0.44	1.08	0.22
FSMC	k_1	11	18	11
	k_2	0.44	1.08	0.22
	ρ	0.8	0.8	0.3
	λ	2	2	2

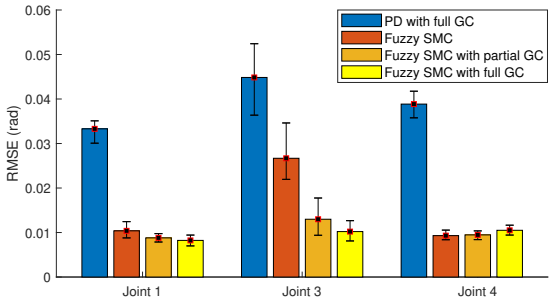

Fig. 8. Bar diagram of the RMSE with variance from 12 trials for each control algorithm.

B. Experiment Results

Experiments were conducted to investigate the effectiveness of the proposed control method. In the tests, the exoskeleton assists the user in performing a complete drinking task, as shown in Fig. 6. Several positions in the operational space were predefined via human demonstration. Then the trajectories were generated in the joint space for the specific task, either eating or drinking, and the human-exoskeleton system was driven to follow the reference joint trajectories. The drinking task is repeated for 12 trials for each control method. During each trial, the weight of the bottle varies from 0.4-0.65kg due to water consumption.

In the first test case, the PD controller with full gravity compensation (which includes gravity compensation for the exoskeleton and the human arm, excluding the payload) was used for the joint trajectory tracking, in which the user was totally passive and forced to follow the desired joint trajectories. The parameters selected for the PD controller as well as FSMC are shown in Table II. The tuning of PD and FSMC follows the procedure as explained in Section III.

The trajectory tracking performance of PD with full gravity compensation was not satisfactory, as shown in Fig. 7(a). The tracking performance of all joints represented by the root mean square error (RMSE) from the 12 trials is shown in Fig. 8 and the detailed statistics are listed in Table III. It is noted that the PD control shows average RMSE values of 0.0333rad, 0.0448rad, and 0.0389 for the three joints, respectively. Moreover, the variations in the RMSE values among 12 trials were also very high, which showed that the controller was not able to handle the uncertain dynamics and external disturbances during different trials.

In the second case, the proposed PD based FSMC was investigated. The results are shown in Fig. 7 (b). From Fig. 8 it can be seen that the tracking performance was significantly improved for each joint of the exoskeleton robot, and the average RMSE values were found to be 0.0104rad, 0.0267rad, and 0.0093rad for joints 1, 3 and 4 respectively. Furthermore, the variation of RMSE for each joint was also reduced, which shows that FSMC has the capability of handling uncertain dynamics and external disturbances.

The performance of FSMC was found better than that of PD with full gravity compensation. To further study the effect of gravity compensation with FSMC, FSMC with partial gravity compensation (gravity compensation for the exoskeleton, excluding human arm and payload) and with full gravity compensation were also considered. The results for these two control methods are demonstrated in Figs. 7(c) and 7(d).

For FSMC with partial gravity compensation, from Fig. 8 and Table III one can see that the tracking performance was improved when compared to the performance with FSMC only, which indicates that the control performance of FSMC can be further improved by combining with partial gravity compensation.

Comparing FSMC with full gravity compensation against that with partial gravity compensation, we can see that their control performance is quite similar: the average RMSE values of joints 1 and 3 were slightly reduced, while the average RMSE value of joint 4 increased slightly. Hence it can be concluded that in the proposed PD based FSMC with gravity compensation, full gravity compensation is not necessary due to several different control methods combined in our approach to improve the tracking performance. Considering the difficulty to have accurate full gravity compensation as discussed in Section V(A), the method of FSMC with partial gravity compensation is suitable and applicable in practical ADL tasks.

VI. CONCLUSIONS

The objective of this work is to assist severely injured people or aged people in ADL by developing a wheelchair exoskeleton. A control approach combining PD control, sliding mode control, and fuzzy logic control is proposed. The approach inherits the advantages of the quick response and stability from the PD control and the robustness from sliding mode control against system uncertainties and external disturbances. Furthermore, the chattering phenomenon caused by classical sliding mode control is eliminated by combining with the fuzzy logic control. The effectiveness of the proposed method and the tracking accuracy are verified by simulations and experiments against two other developed methods. In particular, it is shown that the proposed control method is appropriate for performing real-world ADL tasks such as drinking.

In the future work, we will engage a camera system to detect the motions of the human arm and the locations of the object, to make the whole assistive task more intelligent and autonomous. The EEG/EMG signals will also be investigated to achieve more advanced rehabilitation and assistive control.

This article has been accepted for publication in a future issue of this journal, but has not been fully edited. Content may change prior to final publication. Citation information: DOI 10.1109/TMECH.2020.2983520, IEEE/ASME Transactions on Mechatronics

TABLE III
STATISTICAL ANALYSIS OF CONTROL ALGORITHMS WITH RMSE VALUES (RAD).

Control Algorithm	Exoskeleton Joints	Min RMSE	Max RMSE	Average RMSE	Variance of RMSE
PD with gravity compensation	Joint 1	0.0301	0.0351	0.0333	0.0050
	Joint 3	0.0364	0.0524	0.0448	0.0160
	Joint 4	0.0358	0.0418	0.0389	0.0060
Fuzzy SMC	Joint 1	0.0088	0.0124	0.0104	0.0036
	Joint 3	0.0219	0.0346	0.0267	0.0127
	Joint 4	**0.0084**	0.0105	**0.0093**	0.0021
Fuzzy SMC with partial gravity compensation	Joint 1	0.0079	0.0097	0.0088	**0.0018**
	Joint 3	0.0094	0.0178	0.0130	0.0084
	Joint 4	**0.0084**	**0.0104**	0.0095	**0.0020**
Fuzzy SMC with full gravity compensation	Joint 1	**0.0070**	**0.0094**	**0.0082**	0.0024
	Joint 3	**0.0081**	**0.0127**	**0.0102**	**0.0046**
	Joint 4	0.0094	0.0117	0.0105	0.0023

The best values for all joints are emphasized in boldface.

APPENDIX I

$$
\begin{aligned}
m_{11} &= (c\theta_1 c\theta_2 c\theta_3 - s\theta_1 s\theta_3)c\theta_4 - (c\theta_1 c\theta_2 s\theta_3 + s\theta_1 c\theta_3)s\theta_4 \\
m_{12} &= -(c\theta_1 c\theta_2 c\theta_3 - s\theta_1 s\theta_3)s\theta_4 - (c\theta_1 c\theta_2 s\theta_3 + s\theta_1 c\theta_3)c\theta_4 \\
m_{13} &= c\theta_1 s\theta_2 \\
m_{21} &= (s\theta_1 c\theta_2 c\theta_3 + c\theta_1 s\theta_3)c\theta_4 - (s\theta_1 c\theta_2 s\theta_3 - c\theta_1 c\theta_3)s\theta_4 \\
m_{22} &= -(s\theta_1 c\theta_2 c\theta_3 + c\theta_1 s\theta_3)s\theta_4 - (s\theta_1 c\theta_2 s\theta_3 - c\theta_1 c\theta_3)c\theta_4 \\
m_{23} &= s\theta_1 s\theta_2 \\
m_{31} &= -s\theta_2 c\theta_3 c\theta_4 + s\theta_2 s\theta_3 s\theta_4 \\
m_{32} &= s\theta_2 c\theta_3 s\theta_4 + s\theta_2 s\theta_3 c\theta_4 \\
m_{33} &= c\theta_2 \\
n_{14} &= L_f[(c\theta_1 c\theta_2 c\theta_3 - s\theta_1 s\theta_3)c\theta_4 - (c\theta_1 c\theta_2 s\theta_3 + s\theta_1 c\theta_3)s\theta_4] \\
&\quad + L_u(c\theta_1 c\theta_2 c\theta_3 - s\theta_1 s\theta_3) \\
n_{24} &= L_f[(s\theta_1 c\theta_2 c\theta_3 + c\theta_1 s\theta_3)c\theta_4 - (s\theta_1 c\theta_2 s\theta_3 - c\theta_1 c\theta_3)s\theta_4] \\
&\quad + L_u(s\theta_1 c\theta_2 c\theta_3 + c\theta_1 s\theta_3) \\
n_{34} &= -L_f(s\theta_2 c\theta_3 c\theta_4 - s\theta_2 s\theta_3 s\theta_4) - L_u s\theta_2 c\theta_3
\end{aligned}
$$

APPENDIX II

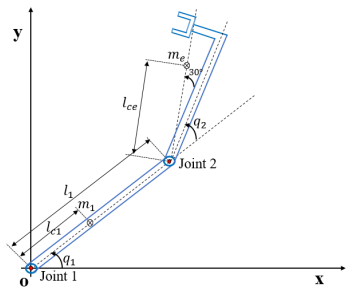

Fig. 9. 2-DOF serial manipulator.

The value of parameters in Fig. 9 and the 2-DOF manipulator dynamic system (20) are given as: $m_1 = 1kg$, $m_e = 2kg$, $l_1 = 1m$, $l_{c1} = 0.5m$, $l_{ce} = 0.25m$, $F_{c1} = 5Nm$, $F_{c2} = 5Nm$, $v_1 = 5.5kgm^2/s$, $v_2 = 2.7kgm^2/s$, $I_1 = 0.12kgm^2$, $I_2 = 0.25kgm^2$, $a_1 = 2.745kgm^2$, $a_2 = 0.375kgm^2$, $a_3 = 0.433kgm^2$, $a_4 = 0.25kgm^2$.

APPENDIX III

TABLE IV
MECHANICAL PROPERTIES OF EXOSKELETON AND ANTHROPOMORPHIC PARAMETERS OF A HUMAN SUBJECT FOR GRAVITY COMPENSATION.

Link	Exoskeleton		Human subject	
	Length (m)	Weight (kg)	Length (m)	Weight (kg)
Upper arm	0.33	1.39	0.33	1.386
Forearm	0.17	0.307	0.37	0.886

REFERENCES

[1] S. Bai, G. S. Virk, and T. Sugar, *Wearable Exoskeleton Systems: Design, Control and Applications*. Institution of Engineering and Technology, 2018.

[2] L. Zhou, W. Chen, J. Wang, S. Bai, H. Yu, and Y. Zhang, "A novel precision measuring parallel mechanism for the closed-loop control of a biologically inspired lower limb exoskeleton," *IEEE/ASME Trans. Mechatronics*, vol. 23, no. 6, pp. 2693–2703, Dec. 2018.

[3] T. Otsuka, K. Kawaguchi, H. Kawamoto, and Y. Sankai, "Development of upper-limb type HAL and reaching movement for meal-assistance," in *Proc. IEEE Int. Conf. Robot. Biomimetics*, pp. 883–888, Dec. 2011.

[4] M. Hessinger, R. Müller, R. Werthschützky, and P. Pott, "Tool position control of an upper limb exoskeleton for robot-assisted surgery," in *Proc. 9th IFAC Symp. on Biol. and Med. Syst.*, pp. 195–200, 2015.

[5] N. Sylla, V. Bonnet, F. Colledani, and P. Fraisse, "Ergonomic contribution of ABLE exoskeleton in automotive industry," *Int. J. Ind. Ergon.*, vol. 44, no. 4, pp. 475–481, 2014.

[6] T. Proietti, V. Crocher, A. Roby-Brami, and N. Jarrassé, "Upper-limb robotic exoskeletons for neurorehabilitation: A review on control strategies," *IEEE Rev. in Biomed. Eng.*, vol. 9, pp. 4–14, 2016.

[7] T. Shibata and T. Murakami, "Null space motion control by PID control considering passivity in redundant manipulator," *IEEE Trans. Ind. Informat.*, vol. 4, no. 4, pp. 261–270, Nov. 2008.

[8] J. Baek, M. Jin, and S. Han, "A new adaptive sliding-mode control scheme for application to robot manipulators," *IEEE Trans. Ind. Electron.*, vol. 63, no. 6, pp. 3628–3637, Jun. 2016.

[9] C. M. Lim and T. Hiyama, "Application of fuzzy logic control to a manipulator," *IEEE Trans. Robot. Automat.*, vol. 7, no. 5, pp. 688–691, Oct. 1991.

[10] Y. Gao, M. J. Er, and S. Yang, "Adaptive control of robot manipulators using fuzzy neural networks," *IEEE Trans. Ind. Electron.*, vol. 48, no. 6, pp. 1274–1278, Dec. 2001.

[11] T. P. d. Nascimento, G. F. Basso, C. E. T. Dórea, and L. M. G. Gonçalves, "Perception-driven motion control based on stochastic nonlinear model predictive controllers," *IEEE/ASME Trans. Mechatronics*, vol. 24, no. 4, pp. 1751–1762, Aug. 2019.

[12] S. Li, X. Yu, L. Fridman, Z. Man, and X. Wang, *Advances in Variable Structure Systems and Sliding Mode Control-Theory and Applications*, vol. 115. Springer, 2017.
[13] M. H. Rahman, M. Saad, J. P. Kenné, and P. S. Archambault, "Nonlinear sliding mode control implementation of an upper limb exoskeleton robot to provide passive rehabilitation therapy," in *Proc. Int. Conf. Intell. Robot. and Appli.*, pp. 52–62, 2012.
[14] A. L'Afflitto, R. B. Anderson, and K. Mohammadi, "An introduction to nonlinear robust control for unmanned quadrotor aircraft: How to design control algorithms for quadrotors using sliding mode control and adaptive control techniques," *IEEE Control Syst.*, vol. 38, no. 3, pp. 102–121, Jun. 2018.
[15] M. Zeinali and L. Notash, "Adaptive sliding mode control with uncertainty estimator for robot manipulators," *Mech. Mach. Theory*, vol. 45, no. 1, pp. 80–90, 2010.
[16] L. Teng, Y. Wang, W. Cai, and H. Li, "Fuzzy model predictive control of discrete-time systems with time-varying delay and disturbances," *IEEE Trans. Fuzzy Syst.*, vol. 26, no. 3, pp. 1192–1206, Jun. 2018.
[17] L. Teng, Y. Wang, W. Cai, and H. Li, "Robust fuzzy model predictive control of discrete-time Takagi-Sugeno systems with nonlinear local models," *IEEE Trans. Fuzzy Syst.*, vol. 26, no. 5, pp. 2915–2925, Oct. 2018.
[18] L. Teng, Y. Wang, W. Cai, and H. Li, "Efficient robust fuzzy model predictive control of discrete nonlinear time-delay systems via Razumikhin approach," *IEEE Trans. Fuzzy Syst.*, vol. 27, no. 2, pp. 262–272, Feb. 2019.
[19] H. Zhou, H. Deng, and J. Duan, "Hybrid fuzzy decoupling control for a precision maglev motion system," *IEEE/ASME Trans. Mechatronics*, vol. 23, no. 1, pp. 389–401, Feb. 2018.
[20] C. Fu, A. Sarabakha, E. Kayacan, C. Wagner, R. John, and J. M. Garibaldi, "Input uncertainty sensitivity enhanced nonsingleton fuzzy logic controllers for long-term navigation of quadrotor UAVs," *IEEE/ASME Trans. Mechatronics*, vol. 23, no. 2, pp. 725–734, Apr. 2018.
[21] M. Van, "An enhanced robust fault tolerant control based on an adaptive fuzzy PID-nonsingular fast terminal sliding mode control for uncertain nonlinear systems," *IEEE/ASME Trans. Mechatronics*, vol. 23, no. 3, pp. 1362–1371, Jun. 2018.
[22] S. Chen, H. Chiang, T. Liu, and C. Chang, "Precision motion control of permanent magnet linear synchronous motors using adaptive fuzzy fractional-order sliding-mode control," *IEEE/ASME Trans. Mechatronics*, vol. 24, no. 2, pp. 741–752, Apr. 2019.
[23] C. S. Chin and W. P. Lin, "Robust genetic algorithm and fuzzy inference mechanism embedded in a sliding-mode controller for an uncertain underwater robot," *IEEE/ASME Trans. Mechatronics*, vol. 23, no. 2, pp. 655–666, Apr. 2018.
[24] Y.-R. Hwang and M. Tomizuka, "Fuzzy smoothing algorithms for variable structure systems," *IEEE Trans. Fuzzy Syst.*, vol. 2, no. 4, pp. 277–284, Nov. 1994.
[25] J. C. Wu and T. S. Liu, "A sliding-mode approach to fuzzy control design," *IEEE Trans. Contr. Syst. Technol.*, vol. 4, no. 2, pp. 141–151, Mar. 1996.
[26] Q. Wu, X. Wang, B. Chen, and H. Wu, "Design and fuzzy sliding mode admittance control of a soft wearable exoskeleton for elbow rehabilitation," *IEEE Access*, vol. 6, pp. 60 249–60 263, 2018.
[27] M. Rahmani and M. H. Rahman, "An upper-limb exoskeleton robot control using a novel fast fuzzy sliding mode control," *J. Intell. Fuzzy Syst.*, vol. 36, no. 3, pp. 2581–2592, 2019.
[28] S. Christensen and S. Bai, "Kinematic analysis and design of a novel shoulder exoskeleton using a double parallelogram linkage," *J. Mech. Robot.*, vol. 10, no. 4, p. 041008, 2018.
[29] B. Siciliano and O. Khatib, *Springer Handbook of Robotics*. Springer, 2016.
[30] B. Siciliano, L. Sciavicco, L. Villani, and G. Oriolo, *Robotics: Modelling, Planning and Control*. Springer, 2010.

Long Teng (S'17-M'18) received the B.Eng. degree in automation from China Jiliang University, Hangzhou, China, in 2010, the M.Eng. degree in automation science and electrical engineering from Beihang University, Beijing, China, in 2013, and the Ph.D. degree in electrical engineering from Nanyang Technological University, Singapore, in 2018. After graduation, he worked with a commercial satellite company in Singapore and a startup for assistive robots in Shenzhen, China, respectively. He is a postdoctoral research fellow with the Department of Materials and Production, Aalborg University, Aalborg, Denmark. His current research interests include human-robot interaction, exoskeleton robots, human intention detection for assistive robots, control system theory and application to robotics, and machine learning with applications to assistive robots.

Muhammad Ahsan Gull (S'19) received the B.Eng. degree in mechatronics engineering from University of Engineering and Technology, Pakistan, in 2012, and received MS degree in mechatronics engineering from National University of Sciences and Technology (NUST), Islamabad, Pakistan in 2015. He served NUST as a lecturer for 2.5 years and now working as a PhD fellow at Department of Materials and Production, Aalborg University, Aalborg, Denmark.

His current research interests include human-robot interaction, exoskeleton robot and application to robotics.

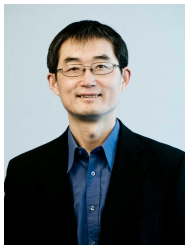

Shaoping Bai (M'01-SM'18) received PhD degree in Robotics from Nanyang Tech. Univ. (NTU), Singapore, 2001. He is currently a professor at Dept. of Materials and Production, Aalborg University, Denmark. His research areas include mechanism theory and novel mechanisms, medical and assistive robots, parallel kinematics machines, with special interest in kinematics, dynamics, linkage and manipulator analysis and synthesis, human-robot interaction modelling and control.

He has served as editor of a number of books, conference proceedings and editorial board of several journals, including ASME J. Mechanisms and Robotics, IEEE Robotics and Automation Letters, among others.